Regional Flood Risk Projections under Climate Change

SANJIB SHARMA,[a,b] MICHAEL GOMEZ,[b] KLAUS KELLER,[a,c,d] ROBERT E. NICHOLAS,[a,e] AND ALFONSO MEJIA[b]

[a] *Earth and Environmental Systems Institute, The Pennsylvania State University, University Park, Pennsylvania*
[b] *Department of Civil and Environmental Engineering, The Pennsylvania State University, University Park, Pennsylvania*
[c] *Department of Geosciences, The Pennsylvania State University, University Park, Pennsylvania*
[d] *Thayer School of Engineering, Dartmouth College, Hanover, New Hampshire*
[e] *Department of Meteorology and Atmospheric Science, The Pennsylvania State University, University Park, Pennsylvania*

(Manuscript received 15 October 2020, in final form 7 June 2021)

ABSTRACT: Flood-related risks to people and property are expected to increase in the future due to environmental and demographic changes. It is important to quantify and effectively communicate flood hazards and exposure to inform the design and implementation of flood risk management strategies. Here we develop an integrated modeling framework to assess projected changes in regional riverine flood inundation risks. The framework samples climate model outputs to force a hydrologic model and generate streamflow projections. Together with a statistical and hydraulic model, we use the projected streamflow to map the uncertainty of flood inundation projections for extreme flood events. We implement the framework for rivers across the state of Pennsylvania, United States. Our projections suggest that flood hazards and exposure across Pennsylvania are overall increasing with future climate change. Specific regions, including the main stem Susquehanna River, lower portion of the Allegheny basin, and central portion of Delaware River basin, demonstrate higher flood inundation risks. In our analysis, the climate uncertainty dominates the overall uncertainty surrounding the flood inundation projection chain. The combined hydrologic and hydraulic uncertainties can account for as much as 37% of the total uncertainty. We discuss how this framework can provide regional and dynamic flood-risk assessments and help to inform the design of risk-management strategies.

KEYWORDS: Hydrology; Climate prediction; Communications/decision making; Flood events; Risk assessment

1. Introduction

Floods drive major damages to communities across the globe, with an estimated annual average loss of U.S. $104 billion (UNISDR 2015). These impacts are expected to rise in the future as the climate is changing and urbanization is changing exposure (Alfieri et al. 2015; Hirabayashi et al. 2013; Wing et al. 2018; Winsemius et al. 2016). There is increasing interest in improving the understanding and quantification of future flood hazards in a changing climate (Judi et al. 2018; Gangrade et al. 2020; FSF 2020). There is also growing recognition of the critical need to enhance the communication of flood hazards and its associated uncertainties to inform stakeholders and the design and implementation of flood risk management strategies (Collet et al. 2018; Kundzewicz et al. 2018; Sanders et al. 2020). The design of flood-risk management strategies can be improved by information about future flood hazards that is based on the best current understanding of the future climate system (Alfonso et al. 2016; Sorribas et al. 2016; Srikrishnan et al. 2019; Zarekarizi et al. 2020).

In the United States, the Federal Emergency Management Agency (FEMA) is responsible for producing Flood Insurance Rate Maps (FIRMs) specifying the boundaries of zones deemed to be most vulnerable to fluvial and coastal flooding (FEMA 2019). The most common delineations are the 100- and 500-yr floodplain boundary, which depict the inundation extent for floods assessed to have a 1% and 0.2%, respectively, chance of being reached or exceeded in any given year. These estimates are widely used by federal, state, and local agencies in the United States for setting national-level flood insurance requirements and managing development in the floodplain at the community level (FEMA 2019).

The FEMA flood maps can provide very useful information, but they are also subject to several limitations (Bales and Wagner 2009; Merwade et al. 2006, 2008; Pappenberger et al. 2005, 2006). For one, they do not account for uncertainties associated with the estimation and mapping of flood inundation (Merwade et al. 2008; Lin et al. 2013) and assume that the flood-event time series is stationary (Villarini et al. 2009). Historical records often reveal nonstationarity due to multiple factors such as changes in precipitation patterns, land cover alterations, and water transfers, among others (Jovanovic et al. 2016, 2017, 2018). Here we design, test, and discuss a framework to derive probabilistic flood inundation projections that accounts for key nonstationarities associated with climate change.

Flood risk can be assessed in terms of hazard, exposure, and vulnerability (Arnell and Gosling 2014; Hirabayashi et al. 2013; Ruhi et al. 2018; Wing et al. 2018; Keller et al. 2020). Hazard refers to the nature, magnitude, and probability of a flood event. Exposure in this case characterizes factors such as the population and value of assets within the floodplain that are likely to experience flooding. Vulnerability characterizes how sensitive the impacts are for a given hazard and exposure. A sound understanding of these risk drivers is important to inform the design of risk management strategies, for example, deciding when and where to acquire land, or floodproofing

Supplemental information related to this paper is available at the Journals Online website: https://doi.org/10.1175/JHM-D-20-0238.s1.

Corresponding author: Alfonso Mejia, aim127@psu.edu

DOI: 10.1175/JHM-D-20-0238.1

infrastructure. Past flood risk assessments have focused on the global scale (Alfieri et al. 2017; Hirabayashi et al. 2013; Jongman et al. 2015; Winsemius et al. 2016; Ward et al. 2015), continental scale (Alfieri et al. 2015; Feyen et al. 2012; Wing et al. 2018), or local watershed scale (Cheng et al. 2017; Dibike and Coulibaly 2005; Dobler et al. 2012; Wu et al. 2014). Recently, Wing et al. (2018) presented estimates of current and future flood risk across the United States. This study finds that nearly 41 million of the U.S. population live within the 1% annual exceedance probability floodplain (compared to only 13 million when calculated using the FEMA flood maps). This difference is largely due to the inclusion of small streams by Wing et al. (2018) that have not been mapped by FEMA. The future flood risk estimates by Wing et al. (2018) do not account for future climate projections. These estimates were recently expanded by Bates et al. (2021) to include future climate projections and multiple types of flooding—fluvial, pluvial, and coastal. However, they did not try to quantify the key sources of uncertainty in flood inundation projections. In addition, most hydrological responses to extreme events are highly regional, and water resources management is often carried out at river basin scales (Hattermann et al. 2017; Varis et al. 2004). Local decision-making scales require local information (Aich et al. 2016; Collet et al. 2018; Demaria et al. 2016; Huang et al. 2013; de Moel et al. 2015).

The main objective of this study is to develop an integrated hydroclimatic modeling framework to assess regional flood hazards and exposure for future climatic conditions. The framework combines five main components: 1) statistically downscaled daily precipitation and near-surface temperature projections (Pierce et al. 2014); 2) the National Oceanic and Atmospheric Administration's (NOAA) Hydrology Laboratory–Research Distributed Hydrologic Model (HL-RDHM) (Koren et al. 2004); 3) the Generalized Pareto distribution (GPD)-based extreme value model (Coles 2001); 4) the LISFLOOD-FP hydraulic model (Neal et al. 2012); and 5) a uncertainty quantification methods applied to these components. The framework involves hydrologic modeling driven by climate ensembles to generate streamflow projections; statistical modeling to estimate flood peaks; hydraulic modeling to estimate water surface elevations; terrain analysis to map the inundation extents; and uncertainty decomposition to quantify the key uncertainty sources in flood inundation projections. We implement this integrated hydroclimatic modeling framework for a regional-scale case study to analyze two interrelated questions: 1) How does climate change alter regional flood hazard and exposure projections? and 2) What drives the total uncertainty in flood inundation projections? In this study, we focus on the hazard and exposure components of flood risk.

Flood inundation projections are subject to multiple sources of uncertainty. These sources include projections of future climate, as well as hydrologic and hydraulic modeling. Previous studies highlight the dominating influence of climate model–driven uncertainty relative to the total uncertainty in extreme flood projections (Hirabayashi et al. 2013; Vetter et al. 2017). Most studies focus on quantifying individual sources of uncertainties in extreme flood projections (Bosshard et al. 2013; Qi et al. 2016), and are silent on the relation between individual sources of uncertainty and the total uncertainty of flood inundation projections (Kim et al. 2019). In addition, previous studies often ignore the effects of hydraulic modeling and mapping on flood inundation extents when assessing climate change impacts on flood projections (Bosshard et al. 2013; Kim et al. 2019). Thus, the relative contribution of hydraulic uncertainty to the total flood inundation projection uncertainty is often unknown. Here we quantify key uncertainties in the flood inundation projection chain, including uncertainties in climate model outputs, hydrologic and hydraulic modeling for a case study.

To implement the proposed modeling framework, we assess flood hazards and exposure across the state of Pennsylvania, which is located in the Mid-Atlantic region of the United States. Flooding has been the most frequent and most damaging natural disaster in Pennsylvania (PEMA 2017), causing an average $92 million loss a year during 1996 and 2014 (USDOE 2015). Regionally, there is strong evidence of rising temperatures, altered precipitation patterns (Hayhoe et al. 2018; Shortle et al. 2015), and increasing intensity of flood events (Sagarika et al. 2014; Zhang et al. 2010). Historical climate records show that temperatures in Pennsylvania have already increased by more than 1.8°F since the early twentieth century (Shortle et al. 2015). Similarly, average annual precipitation in Pennsylvania has increased by approximately 10% over the past 100 years and, by 2050, it is expected to increase by 8% (Kang and Sridhar 2018; Shortle et al. 2015). There has been an increase in the frequency and magnitude of damaging flood occurrence in communities across Pennsylvania. For instance, the most destructive floods in the Susquehanna and Delaware River basins have occurred in recent years, each associated with different flood-generating mechanisms: Hurricane Ivan (September 2004), late winter–early spring extratropical systems (April 2005), warm-season convective systems (June 2006), and tropical storm Lee (September 2011) (Armstrong et al. 2014; Smith et al. 2010, 2011). There is a critical need to better understand future flood risks in Pennsylvania (Iulo et al. 2020).

The remainder of the paper is organized as follows. Section 2 presents the methods used in this study. The main results and their implications are examined in section 3. Last, section 4 summarizes key findings.

2. Materials and methods

We develop and implement an integrated hydroclimatic modeling framework consisting of downscaled climate model outputs, a hydrologic model, a nonstationary extreme value model, a hydraulic model, and uncertainty quantification (Fig. 1). The proposed framework uses downscaled climate projections for precipitation and temperature to force the NOAA's HL-RDHM (Koren et al. 2004) resulting in future projected streamflow at selected gauged locations in Pennsylvania. The projected streamflow is statistically postprocessed to compute extreme flows with 100-yr return periods. The 100-yr flood peaks are used as boundary conditions to the hydraulic model LISFLOOD-FP (Bates et al. 2013) to generate flood inundation projections. Finally, the flood inundation projections are used to analyze flood

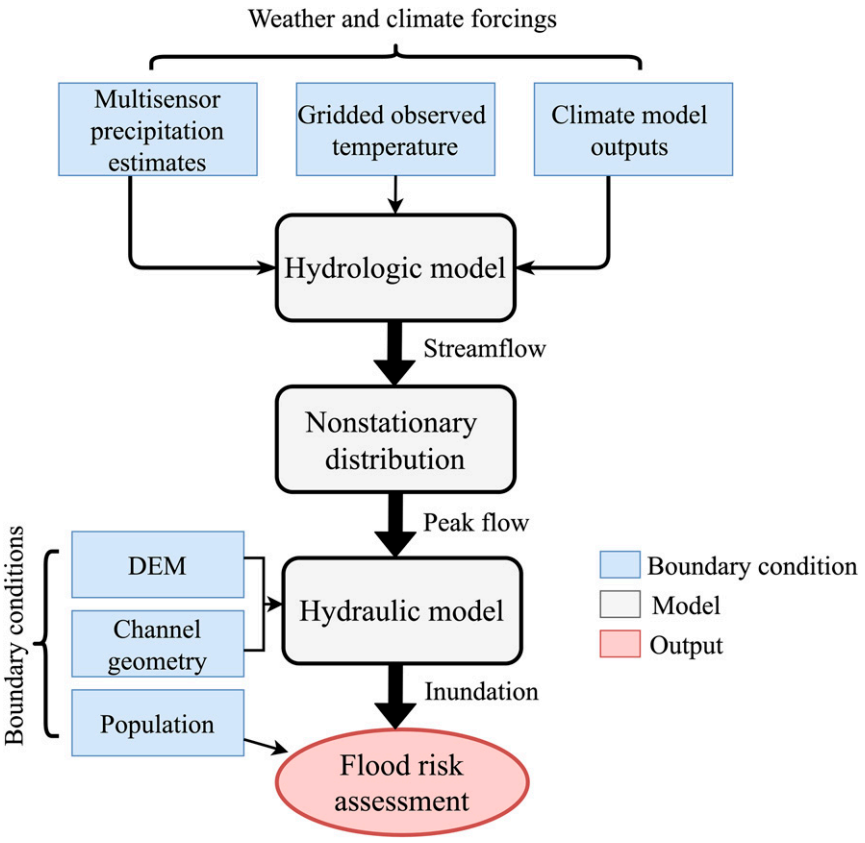

FIG. 1. Flowchart illustrating the general methodological approach for flood inundation risk projections. The approach starts with the climate model outputs, which are used to drive the hydrologic model and generate streamflow projections. Together with the statistical and hydraulic model, the projected streamflow is then used to map the uncertainty of flood inundation projections for extreme flood events. DEM = digital elevation model.

hazards and exposure. Next, we describe the datasets, models, and techniques involved in our overall workflow (Fig. 1).

a. Datasets

For the observational datasets, we use multisensor precipitation estimates (MPEs), gridded near-surface air temperature, and streamflow observations at selected U.S. Geological Survey (USGS) gauges. These observational datasets are used to calibrate the hydrological model. We use hourly gridded MPEs and near-surface air temperature data at $4 \times 4\,\text{km}^2$ from the NOAA's Middle Atlantic River Forecast Center. Similar to the National Centers for Environmental Prediction's Stage-IV dataset (Prat and Nelson 2015), the MPEs provided by the River Forecast Center represent a continuous time series of hourly, gridded precipitation observations at $4 \times 4\,\text{km}^2$ cells. The gridded near-surface air temperature data at $4 \times 4\,\text{km}^2$ resolution were developed by the River Forecast Center by combining multiple temperature observation networks as described by Siddique and Mejia (2017). We obtained daily streamflow observations for the selected gauged locations from the USGS (https://waterdata.usgs.gov/nwis/rt).

For the climate ensemble, we use the localized constructed analogs (LOCA; Pierce et al. 2014) of daily precipitation and near-surface temperature outputs for 13 general circulation models from the Coupled Model Intercomparison Project CMIP5 datasets. The CMIP5 outputs are for model runs forced by emissions corresponding to Representative Concentration Pathway scenario 8.5 (RCP8.5) (Taylor et al. 2012; Meinshausen et al. 2011). The 13 considered climate models are CESM1-CAM5, CanESM2, EC-EARTH, GFDL-ESM2M, GISS-E2-R, HadGEM2-CC, HadGEM2-ES, IPSL-CM5A-LR, IPSL-CM5A-MR, MPI-ESM-LR, MPI-ESM-MR, BCC-CSM1-1, and INM-CM4 (Table 1). These climate models are selected since they demonstrate improved skill and reliability across the Northeast region (Demaria et al. 2016). The downscaled model outputs are at $6 \times 6\,\text{km}^2$ spatial resolution and provided at https://gdo-dcp.ucllnl.org/downscaled_cmip_projections/dcpInterface.html. We use bilinear interpolation to transform the climate model outputs to the $4 \times 4\,\text{km}^2$ grid cell resolution of the hydrological model.

b. Hydrological model

We use the NOAA's HL-RDHM as the hydrological model (Koren et al. 2004). HL-RDHM is a spatially distributed conceptual model, where the basin system is divided into regularly spaced, square grid cells to sample spatial heterogeneity and variability. We run HL-RDHM at a spatial resolution of $4 \times 4\,\text{km}^2$.

TABLE 1. The 13 models of the Coupled Model Intercomparison Project phase 5 (CMIP5) used in this study.

Modeling center (or group)	Institute ID	Model name
Beijing Climate Center, China Meteorological Administration	BCC	BCC-CSM1.1
Community Earth System Model Contributors	NSF-DOE-NCAR	CESM1-CAM5
Canadian Centre for Climate Modelling and Analysis	CCCMA	CanESM2
EC-EARTH consortium	EC-EARTH	EC-EARTH
NOAA/Geophysical Fluid Dynamics Laboratory	NOAA GFDL	GFDL-ESM2M
NASA Goddard Institute for Space Studies	NASA GISS	GISS-E2-R
Met Office Hadley Centre	MOHC	HadGEM2-CC
Met Office Hadley Centre	MOHC	HadGEM2-ES
Institut Pierre-Simon Laplace	IPSL	IPSL-CM5A-LR
Institut Pierre-Simon Laplace	IPSL	IPSL-CM5A-MR
Max-Planck-Institut für Meteorologie (Max Planck Institute for Meteorology)	MPI-M	MPI-ESM-LR
Max-Planck-Institut für Meteorologie (Max Planck Institute for Meteorology)	MPI-M	MPI-ESM-MR
Institute of Numerical Mathematics	INM	INM-CM4

Within HL-RDHM, we use the Sacramento Soil Moisture Accounting model with Heat Transfer (SAC-HT) to represent hillslope runoff generation, and the SNOW-17 submodel is used to represent snow accumulation and melting. The hillslope runoff, generated at each grid cell by SAC-HT and SNOW-17, is routed to the stream network using a nonlinear kinematic wave algorithm (Koren et al. 2004; Smith et al. 2012). Likewise, we route flows in the stream network downstream using a similar nonlinear kinematic wave algorithm that accounts for parameterized stream cross-section shapes (Smith et al. 2012; Koren et al. 2004). HL-RDHM has successfully been used before to predict and map flood events under a wide range of conditions within our study area (Gomez et al. 2019; Sharma et al. 2018; Siddique and Mejia 2017; Zarzar et al. 2018).

Following previous studies (Koren et al. 2004; Reed et al. 2004), we calibrate HL-RHDM by adjusting a subset of model parameters. Specifically, we select ten out of the 17 SAC-HT parameters based upon prior experience and preliminary parameter sensitivity tests. The adjusted parameters are associated with baseflow, percolation, evaporation, storm runoff and channel routing. To calibrate the selected HL-RDHM parameters, we multiply each a priori parameter field by a factor. It is these multiplying factors that are actually calibrated, not the parameter values in each grid cell. We calibrate the model at the outlet of major river basins in Pennsylvania. Thus, the scaling factors (multipliers) for the nested subbasins within the calibrated ones remain the same. The multiplying factors are adjusted manually first; once the manual changes do not yield noticeable improvements in model performance, the factors are optimized using the automatic technique of stepwise line search (SLS) (Kuzmin 2009; Kuzmin et al. 2008). We use this approach as it is readily available within HL-RDHM and has been shown to provide reliable parameter estimates (Kuzmin 2009; Kuzmin et al. 2008; Sharma et al. 2018; Siddique and Mejia 2017). We optimize the objective function (OF)

$$\mathrm{OF} = \sqrt{\sum_{i=1}^{m} [q_i - s_i(\mathbf{\Omega})]^2}, \tag{1}$$

where q_i and s_i denote the daily observed and simulated flows at time i, respectively; $\mathbf{\Omega}$ is the parameter vector being estimated; and m is the total number of days used for calibration.

To assess the performance of HL-RDHM, we compare the daily simulated flows with daily observed flows from USGS gauges. The model is calibrated during 2008–12 at selected USGS gauge stations for the major river basins in Pennsylvania. We use the year 2007 to spin up the model. We validate the model performance by randomly selecting a set of 26 uncalibrated gauge stations for the same time period of 2008–12. This approach is adopted to ensure the streamflow simulation performance is reasonable for basins with different sizes. We do not calibrate each gauged basin because of computational and time constraints.

We obtain the simulated flows by forcing the model with gridded precipitation and near-surface temperature observations. For calibration, we use 24-hourly precipitation accumulations to force HL-RDHM and generate daily flows. The meteorological datasets used to calibrate the model may not fully resolve the variability of the meteorological forcing. This is an area, together with calibration approaches, of continued improvement.

To assess the quality of the streamflow simulations from HL-RDHM, we employ the modified correlation coefficient (R_m) (McCuen and Snyder 1975) and Nash–Sutcliffe efficiency (NSE) (Nash and Sutcliffe 1970) as performance measures. Overall, the performance of the simulated streamflow is deemed satisfactory at both the calibration and validation gauge stations (Fig. 2). The R_m for the calibration stations is greater than 0.90. Likewise, the NSE ranges from 0.75 to 0.85 for the calibration stations (Fig. 2). The R_m for the validation stations ranges from ~0.80 to 0.95, while the NSE ranges from ~0.60 to 0.75 (Fig. 2).

c. *Nonstationary extreme value analysis of flood events*

Statistical distributions of extreme floods are widely used to inform flood-sensitive infrastructure design, floodplain mapping, risk assessment and environmental management (Bopp et al. 2020; Bracken et al. 2018; Villarini et al. 2009). Traditional approaches for extreme flood estimation use historical records and assume stationarity in streamflow time series (FEMA 2019). In a changing climate, however, traditional approaches can lead to poor hazard estimates (Pralle 2019). Here we compute extreme floods allowing for nonstationary conditions. For this, we use the peak over threshold approach with a Poisson point process parameterization of the GPD (Coles 2001). As

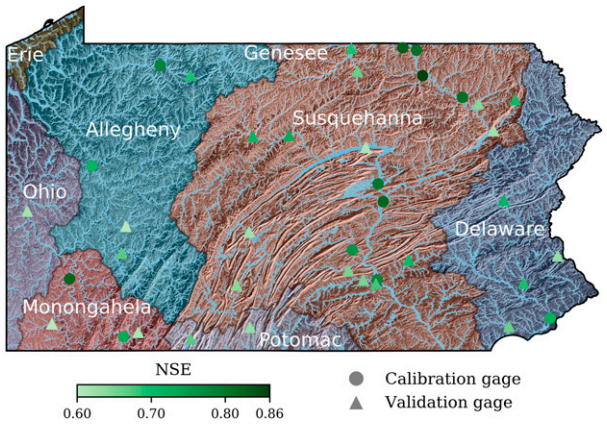

FIG. 2. Map illustrating the major river basins in Pennsylvania. The map also shows the hydrologic model calibration and validation gauge stations, and the corresponding performance of the hydrologic simulations based on the Nash–Sutcliffe efficiency (NSE) index.

opposed to selecting a single peak flood per year, the peak over threshold approach enables us to use daily streamflow data that exceed a specified threshold to fit the GPD model parameters. This approach allows us to consider more information about the extremes. We use a constant threshold μ equal to the 95th percentile of the daily maximum flow (Lang et al. 1999).

The probability density function for the GPD model is defined by

$$f[x(t);\mu(t),\sigma(t),\xi(t)] = \frac{1}{\sigma(t)}\left[1+\xi(t)\frac{x(t)-\mu(t)}{\sigma(t)}\right]^{-\left[\frac{1}{\xi(t)}+1\right]}, \tag{2}$$

where x is the daily streamflow observations for current flood peak estimates or the projected daily streamflow for future flood peaks, σ is the scale parameter that governs the width of the distribution, and ξ is the shape parameter that governs the heaviness of the distribution's tail, all as functions of time t. The Poisson process governs the probability p of observing n exceedances of threshold ? during a time interval Δt:

$$p[n(t);\lambda(t)] = \frac{[\lambda(t)\Delta t]^{n(t)}}{n(t)!}\exp[-\lambda(t)\Delta t], \tag{3}$$

where λ is the Poisson rate parameter. We incorporate potential nonstationary into the GPD model by allowing the model parameters to covary with time (Papoulis and Pillai 2002; Koutsoyiannis 2006) such that

$$\begin{aligned}\lambda(t) &= \lambda_0 + \lambda_1(t),\\ \sigma(t) &= \exp[\sigma_0 + \sigma_1(t)],\\ \xi(t) &= \xi_0 + \xi_1(t),\end{aligned} \tag{4}$$

where λ_0, λ_1, σ_0, σ_1, ξ_0, and ξ_1 are regression parameters. Further, if $\lambda_1 = \sigma_1 = \xi_1 = 0$, the GPD parameters $\lambda(t)$, $\sigma(t)$, and $\xi(t)$ are constant, yielding a stationary statistical model.

We adopt a Bayesian approach and use Markov chain Monte Carlo sampling for parameter estimation (Stephenson and Tawn 2004). This approach combines the knowledge brought by a prior distribution and the observations into the parameters' posterior distribution. We produce 10^5 iterations for one MCMC chain and remove the first 25 000 iterations to account for burn-in. We develop separate GPD models for the period of 1981–2017 and 2020–99 to estimate 100-yr flood peaks in 2017 and 2099, respectively. The stationary GPD model for the period of 1981–2017 is based on historical streamflow observations. The nonstationary GPD model for the period of 2020–99 is based on flow projections obtained by forcing HL-RDHM with the GCM outputs.

d. *Regionalization of the 100-yr flood peaks*

To map the flood extent for an entire region with the LISFLOOD-FP hydraulic model, we need to estimate the 100-yr flood peak for any river location within that region since these estimates are used as boundary conditions by the LISFLOOD-FP. From the flood frequency analysis with the GPD distribution, we obtain estimates of the 100-yr flood peak at selected gauged locations. To regionalize these estimates, we use a scaling relationship between the 100-yr peak Q_p and the drainage area A:

$$Q_p = \beta A^{\alpha}, \tag{5}$$

where β is the proportionality constant and α the scaling exponent. The parameters in Eq. (5) are estimated using ordinary least squares (England et al. 2018; Smith et al. 2011).

e. *Flood inundation mapping*

We use the LISFLOOD-FP hydraulic model (Bates et al. 2013) with the subgrid formulation to simulate and project flood inundations along rivers in Pennsylvania. LISFLOOD-FP is a 2D hydraulic model for subcritical flow that solves the local inertial form of the shallow water equations using a finite difference method on a staggered grid. The model requires as input ground elevation data describing the floodplain topography, channel bathymetry information (river width, depth, and shape), and inflow to the modeling domain as the boundary condition information. To apply LISFLOOD-FP, we use the subgrid-scale hydrodynamic scheme of Neal et al. (2012) to solve the momentum and continuity equations for both channel and floodplain flow. The scheme operates on a rectangular grid mesh of the same resolution as the input DEM, using a finite difference scheme to solve the governing equations. River width and depth are assumed to be uniform along the reach. The cells' water depths are updated using mass fluxes between cells while ensuring mass conservation. To configure LISFLOOD-FP, we use floodplain topography information from the Pennsylvania Spatial Data Access archive (PASDA; https://www.pasda.psu.edu/), and extreme flood events from the nonstationary GPD model and scaling relationship in Eq. (5).

We run LISFLOOD-FP for all rivers in Pennsylvania using a 30-m digital elevation model (DEM) from PASDA. In addition, we use other DEM resolutions, 1 and 10 m, at selected

locations as part of our uncertainty analysis (section 2g). Peak flows with 100-yr return period are used as the inflow boundary condition. Channel bathymetry is estimated using regional, hydraulic-geometry scaling relationships from previous studies (Cinotto 2003; Chaplin 2005; Clune et al. 2018; Roland and Hoffman 2011). This approach is useful when bathymetry data are not available (Mejia and Reed 2011a,b). We use a constant Manning's roughness value of 0.045 for both the channel and floodplain. The chosen Manning's roughness value is similar to values previously used for rivers in Pennsylvania (Newlin and Hayes 2015). Structural flood mitigation barriers, such as levees are not explicitly incorporated into the hydraulic analysis. This decision is made since many levee systems in Pennsylvania are near their design life, and most of these systems have not been properly rehabilitated and were designed using outdated statistical flood estimates (PIRC 2018). Furthermore, it is challenging to evaluate in advance whether levees will perform as intended under current and future climatic conditions, since a levee system's failure may be defined by idiosyncratic causes. An alternative would be to compare model simulations with and without flood mitigation barriers, where levees are incorporated into LISFLOOD-FP following approach by Bates et al. (2021). Such an alternative is outside the scope of this study.

f. *Flood hazards and exposure analysis*

We assess flood hazards and exposure in all cities and boroughs in Pennsylvania for current and projected future climatic conditions. Pennsylvania has 959 boroughs and 56 cities. Boroughs are defined as incorporated political subdivisions and are mostly less populous than cities. Most of the boroughs in Pennsylvania have populations under 5000, though there are some exceptions. Some major cities in Pennsylvania include Philadelphia (with more than one million residents), Pittsburgh, and Scranton.

We characterize flood hazards by the extent of flooding resulting from the 100-yr flood peak. We calculate flood exposure from the population within the flood extent. Flood hazards and exposure are both expressed as percentages. The percent hazard is the flood inundation area standardized to the total area of a city/borough. The percent exposure is the population in the flood inundation area standardized to the total population of a city/borough. We use population from the 2010 U.S. Census Bureau data (U.S. Census Bureau 2010). For a particular borough/city, we disaggregate the total population based on the urban development intensity of each developed grid cell in the 2011 National Land Cover Database (Homer et al. 2012). The National Land Cover Database provides the definitive Landsat-based, 30-m resolution, land cover database for the United States.

g. *Assessing key uncertainties of the flood inundation projections*

To assess key uncertainties in flood inundation projections, we use a cumulative uncertainty approach (Kim et al. 2019). This approach decomposes the total uncertainty to individual uncertainty sources, such that the sum of the uncertainties from individual sources is equal to the total uncertainty in flood inundation projections. We consider uncertainty from three key sources in the flood inundation projection chain: climate, hydrology, and hydraulics. Climate uncertainty in this case is the uncertainty sampled by the information derived from the global climate model runs. Hydrologic uncertainty refers to the uncertainty in the GPD model parameters obtained using Bayesian inference. Hydraulic uncertainty is sampled by the topographic uncertainty due to the choice of different DEM resolutions: 1, 10, and 30 m.

For the uncertainty assessment, we compute the stage uncertainty as the contribution to uncertainty from each of the three stages (climate, hydrology and hydraulic) in the flood inundation projection chain. This analysis samples a relatively small subset of potentially important uncertainties. For example, we sample just a subset of climate models, initial conditions, and climate model parameters (Sriver et al. 2015). Further, the analysis accounts for the hydrologic uncertainty associated with the GPD's parameters while the HL-RDHM model's parameters are fixed. We sample hydraulic uncertainty by considering the topographic uncertainty due to the choice of different DEM resolutions. Such consideration neglects the contribution of potentially important uncertainties, including channel width, channel shape, and channel roughness.

To characterize the stage uncertainty, we first compute the conditional cumulative uncertainty up to a particular stage, which is defined as the variation in the projected flood inundation extent due to the modeling choices up to that stage, while the choices beyond that stage are fixed. For instance, conditional cumulative uncertainty up to the hydrology stage represents the variation in flood inundation projections due to the choice of different GCM outputs and GPD parameters, while the DEM resolution is fixed. Then the marginal cumulative uncertainty up to a particular stage is computed as an average of conditional cumulative uncertainties. Finally, we compute the uncertainty of each stage as the difference between successive marginal cumulative uncertainties.

Specifically, we calculate stage uncertainty as follows. We denote by K the total number of stages in the flood inundation projection chain, in this case $K = 3$ (climate, hydrology, and hydraulic stage). For a particular stage k, there are χ_k models/scenarios. The cumulative uncertainty up to stage k is defined as the variation in the projected values due to the choice of models/scenarios up to stage k, while the models/scenarios after stage k are fixed. The cumulative uncertainty up to stage k is denoted by $U^{\text{cum}}(\chi_1, \ldots, \chi_k)$. For the specific models/scenarios of stage k, we let $P(x_1, x_2, \ldots, x_K)$ be the projected value using the models/scenarios x_k, $k = 1, \ldots, K$. For a given model/scenario after stage k, the set of projected values are

$$q_{x_{k+1},\ldots,x_K} = [P(x_1, \ldots, x_k, x_{k+1}, \ldots, x_K): x_j \in \chi_j, j = 1, \ldots, k]. \tag{6}$$

Then $U^{\text{cum}}(q_{x_{k+1},\ldots,x_K})$ can be interpreted as the conditional cumulative uncertainty up to stage k while the models/scenarios after stage k are fixed as $x_{k+1}, \ldots, x_K$. The marginal cumulative

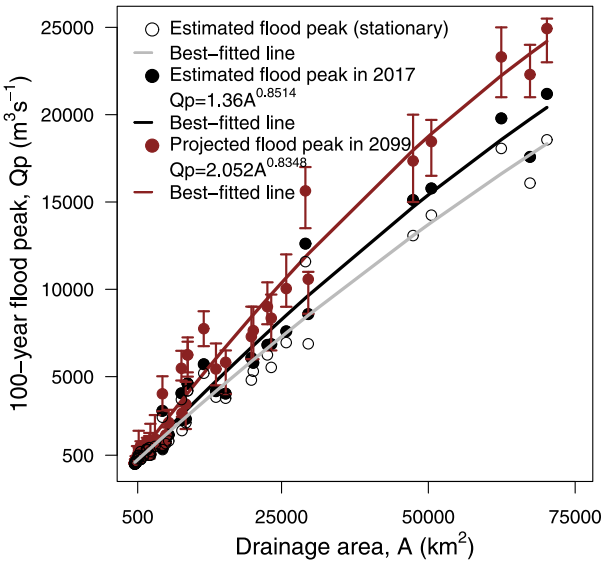

FIG. 3. Scaling of the 100-yr flood peak with the drainage area for locations in Pennsylvania. The scaling relationship is shown for current (2017) and projected flood peak estimates (2099). Flood peak estimates for year 2017 are based on the historical flood records under the stationary and nonstationary assumption. The flood peaks for 2099 depict the mean flood projections, and the corresponding error bar represents the maximum and minimum projected flood peak. The solid lines represent the best fit line under the stationary assumption (gray line) as well as the nonstationary assumption in 2017 (black line) and 2099 (brown line).

uncertainty up to stage k is the average of conditional cumulative uncertainties defined as

$$U^{\text{cum}}(\chi_1,\ldots,\chi_k)=\frac{1}{\prod_{j=k+1}^{K} n_j}\sum_{x_{k+1}\in\chi_{k+1}}\cdots\sum_{x_K\in\chi_K}U(q_{x_{k+1},\ldots,x_k}). \quad (7)$$

Since the cumulative uncertainty increases monotonically (Kim et al. 2019), we can define the uncertainty of each stage as the difference between successive cumulative uncertainties. That is, the uncertainty of stage k, denoted by $U^{\text{cum}}(\chi_k)$, is defined as

$$U^{\text{cum}}(\chi_k)=U^{\text{cum}}(\chi_1,\ldots,\chi_k)-U^{\text{cum}}(\chi_1,\ldots,\chi_{k-1}). \quad (8)$$

The uncertainty of each stage is the amount of contribution to the cumulative uncertainty. Also, the sum of uncertainties of individual stages is always equal to the total uncertainty $U^{\text{cum}}(\chi_1,\ldots,\chi_k)$. The uncertainty of stage k can also be defined as the sum of the variation of the main effect of stage k and the variations of the interactions between stage k and stages after k.

The stage uncertainty and cumulative uncertainty are both expressed in terms of the range (Chen et al. 2011) and standard deviation (Bosshard et al. 2013) of the projected flood inundation extents. For a real number $y=q_{x_{k+1},\ldots,x_K}$ and a set of $y\{y_1,\ldots,y_n\}$, the range and standard deviation are defined as

$$\text{range}=\max_{1\le i\le n}y_i-\min_{1\le i\le n}y_i, \quad (9)$$

$$\text{standard deviation}=\frac{1}{n}\sum_{i=1}^{n}(y_i-\bar{y}), \quad (10)$$

where $\bar{y}=(1/n)\sum_{i=1}^{n}y_i$.

3. Results and discussion

a. Regional flood frequency analysis

We summarize the results obtained from the regional flood frequency analysis using the scaling relationship between the 100-yr flood peak Q_p and the drainage area A. For years 2017 and 2099, we find that the scaling of the 100-yr flood peaks with drainage area performs reasonably well with a Pearson correlation coefficient R exceeding 0.9 (Fig. 3). The years 2017 and 2099 are used for all our flood risk analyses and results. Figure 3 shows the mean 100-yr flood peak estimates and projections in years 2017 and 2099, respectively, as well as the estimates under the stationary assumption for historical flood records. Flood peak estimates and projections in years 2017 and 2099 are based on the estimated and projected streamflow, respectively, obtained by forcing HL-RDHM with the climate models' outputs.

The nature of the scaling relationships (Fig. 3) has implications for flood-risk management. Based on the power-law fits in Fig. 3, the ratio between the 100-yr flood peak for 2099, $Q_{p,2099}$, and 2017, $Q_{p,2017}$, is $Q_{p,2099}/Q_{p,2017}=1.50A^{-0.0196}$. The ratio of the flood peaks indicates that the drainage area has a small and slightly negative amplification effect on future flood peaks since the value of the scaling exponent for the ratio, −0.0196, is small. The ratio of the flood peaks also shows that the flood-peak amplification associated with climate projections is mainly due to the value of the proportionality constants in the power-law fits. Taken together, these results suggest that future increases in flood peaks from climate projections tend to have a disproportionate effect on smaller basins. Many flood-related management decisions, for example, those associated with stormwater management, are made in smaller basins, which adds urgency to the need of adapting local flood regulations and design standards to account for potentially changing climate conditions. In addition, the regionalized flood frequency approach allows estimating flood peaks in areas with missing or poor quality of records, facilitating the analysis of both gauged and ungauged river and stream networks.

The stationary assumption underestimates the 100-yr flood peaks relative to the nonstationary flood peaks (Fig. 3). In other words: assuming stationary flood peaks can underestimate actual flood hazards in our analysis. For example, the flood hazards further increase with the nonstationary flood peak projections for the year 2099 relative to the 2017 nonstationary flood estimates (Fig. 3). As compared to the flood peak estimates for 2017, the projected flood peak is higher, in terms of absolute values, in the case of larger basins, as implied by the scaling relationships obtained.

b. Flood hazard and exposure from future climatic conditions

Our results suggest that most cities (Figs. 4a,b) and boroughs (Figs. 4c,d) in Pennsylvania are projected to face higher flood

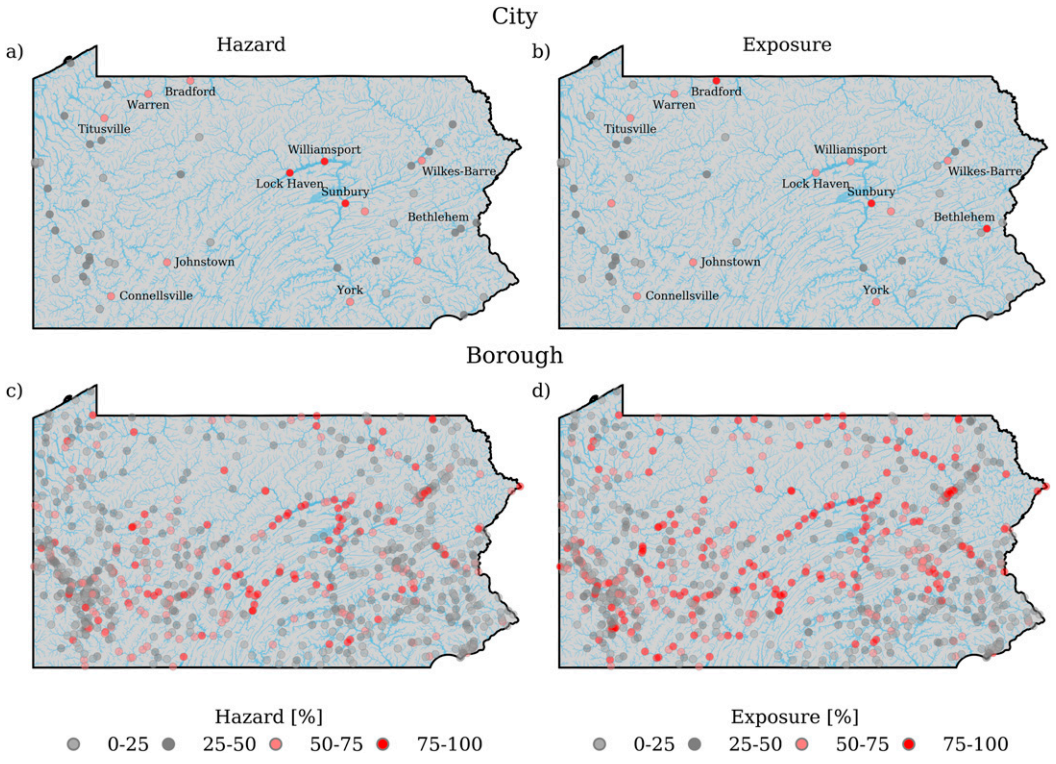

FIG. 4. Projected flood hazard and exposure in year 2099 for all the (a),(b) cities and (c),(d) boroughs in Pennsylvania. Hazard (%) indicates the inundation area standardized to the total area of a city or borough. Exposure (%) indicates the population in the projected flood inundation extents standardized to the total population of a city or borough. There are 959 boroughs and 56 cities in Pennsylvania.

hazards and exposure under future climatic conditions in the year 2099. Populous cities, however, seem to have relatively lower flood hazards and exposure. For instance, the three largest cities (Philadelphia, Pittsburgh, and Scranton) show relatively low projected flood hazards and exposure compared to smaller cities (Figs. 4a,b). Our analysis suggests that these cities have less than 25% projected flood hazards and exposure in 2099.

Some of the cities with the highest projected flood hazards include Sunbury, Williamsport, Lock Haven, Warren, Bradford, Wilkes Barre, Johnstown, York, and Connellsville (Fig. 4a; refer to Table S1 in the online supplemental material). These cities are projected to have more than 50% flood hazards and exposure. The top three cities with the highest projected flood hazards are Lock Haven, Williamsport, and Sunbury (Fig. 4a), which are all located along the West Branch Susquehanna River. Importantly, based on NOAA's National Centers for Environmental Information (NCEI) storm events database (https://www.ncdc.noaa.gov/stormevents/), these three cities have all experienced a substantial number of flood events over time, including events within the last decade, suggesting that our flood hazard metric can capture hotspot areas prone to flooding within Pennsylvania. Specifically, the West Branch Susquehanna River at Williamsport has experienced 40 flood events between 1864 and 2018 (NCEI 2020). Lock Haven has experienced 21 flood events between 1889 and 2010, while Sunbury has experienced 14 flood events between 1936 and 2011 (NCEI 2020). The cities with the highest projected exposure include Bradford, Sunbury, and Bethlehem (Fig. 4b), which are also cities with high flood hazards. Of all the considered cities, Sunbury demonstrates the highest projected flood hazards and exposure (Figs. 4a,b). Sunbury is located at the confluence between the West and North Branch of the Susquehanna River. This makes Sunbury particularly vulnerable to flooding as flood events can occur in either branch of the Susquehanna River (FCSMA 2020).

Boroughs around the high hazards/exposure cities tend to have higher hazards and exposure (Figs. 4c,d). For example, most of the boroughs around the cities of Lock Haven, Williamsport, and Sunbury, and particularly along the West Branch Susquehanna River, show higher flood hazards and exposure. Boroughs along the West Branch Susquehanna River, including Duboistown, Montgomery, Muncy, South Williamsport, Lewisburg, Milton, and Selinsgrove are projected to have more than 50% flood hazards and exposure (refer to Table S2). Neighboring boroughs to the largest metropolitan area (Philadelphia) generally have lower flood hazards and exposure. For example, most of the boroughs around Philadelphia are projected to have less than 25% flood hazards and exposure.

Some of the projected flood hazards and exposure tend to be spatially clustered (Fig. 4). By visually inspecting our flood

hazards and exposure maps (Fig. 4), we identify the most salient clusters. The high hazards and exposure clusters are primarily concentrated along the West Branch of the Susquehanna River, the southwest portion of the Susquehanna basin (also called Juniata subbasin), the lower portion of the Allegheny basin (Figs. 2 and 4), and the central portion of Delaware River basin. The historical records associated with these clusters show that these areas are prone to frequent and severe flooding. For example, the mainstem of the Susquehanna and Delaware River have experienced several devastating floods in past decades, with the four most recent events in the years 2004, 2005, 2006 and 2011 (Gitro et al. 2014; Suro et al. 2009). These historical events caused record to near-record flood crests along most of the streams and rivers throughout the main stem Susquehanna and Delaware River. For instance, for the Susquehanna and Delaware River flood event of 2004, peak discharges on the unregulated reaches remained below a 50-yr recurrence interval, while at the regulated reaches it equaled or exceed the estimated 100-yr recurrence interval (Brooks 2005). Many communities that were flooded during the 2004, 2005, and 2006 floods were again flooded in 2011 (Gitro et al. 2014).

Several factors, including development, stormwater management, floodplain encroachment and reservoir management, have been hypothesized as contributing and exacerbating factors for recent flooding in the Susquehanna and Delaware River basins (Brooks 2005; DRBC 2006). Many of these historical flood events have been caused by different flood generating mechanisms: Hurricane Ivan (September 2004), late winter–early spring extratropical systems (April 2005), warm-season convective systems (June 2006), and Tropical Storm Lee (September 2011) (Smith et al. 2010, 2011). The importance of tropical cyclone projections points to an important caveat as well as a research need. This is because resolving the relevant scales and physical mechanisms is still challenging in climate models (Strachan et al. 2013; Knutson et al. 2015; Gori et al. 2020). Global climate model outputs do not resolve all the weather and climate phenomena relevant to flood-producing rainfall events. Nonetheless, current climate projections, such as CMIP data, provide valuable data to inform flood risk assessments. As global climate models are constantly evolving, it is important to develop flood-risk assessment methodologies that can facilitate the incorporation of climate projection data. This is in part our aim with this regional flood risk approach. An alternative is to employ approaches that statistically combine climate projections with other sources of data, such as tropical storms' simulations, to improve the representation of flood-producing rainfall events not captured by the latest climate projection datasets (Bates et al. 2021).

Our integrated modeling framework enables a quantitative (and approximate) assessment of flood hazards and exposure of cities and boroughs for projected future climatic conditions. Traditionally, flood hazard estimates are only produced under existing conditions using historic flood records to characterize current risks (FEMA 2019). By using GCM projections, we sample key effects of changing climatic conditions to estimate how flood hazards and exposure can change over the decades across cities and boroughs in Pennsylvania. Specifically, we demonstrate a method that leverages an interconnected system of data, models, and analyses to provide nonstationary riverine flood hazard information from local to regional scale. Climate-informed flood hazard projections provide a more complete picture of decision-relevant information for the management of flood risks.

c. *Flood risk from future climatic conditions*

The intersection of flood hazards and exposure informs flood-risk assessments (Arnell and Gosling 2014; Hirabayashi et al. 2013; Ruhi et al. 2018; Wing et al. 2018). Flood risk increases with increasing hazards and exposure. We find a strong correlation ($R > 0.90$) between the projected flood hazards and exposure for boroughs (Fig. 5a) and cities (Fig. 5b). Cities with higher flood hazard tend to result in higher exposure, with cities in the Lehigh Valley such as Bethlehem being an exception (Figs. 4a,b and 5b). For the city of Bethlehem, flood hazard of approximately 40% is projected to result in about 75% of exposure. Bethlehem is one of the most populous cities in Pennsylvania, with development mostly concentrated on both sides of the Lehigh River and Monocacy Creek, which flow through the city. Flood risk in Bethlehem is driven by the compounding effects of floods in the Lehigh River and/or Monocacy Creek. The Lehigh River at Bethlehem has recorded 15 flood events since 1902, while the Lehigh River Valley itself has experienced 129 flood events between 1950 and 2011 (NCEI 2020).

For boroughs (Fig. 5a), the relation between hazards and exposure generally shifts above the one-to-one line, indicating higher exposure for a particular hazard. Increasing exposure with projected flood hazards further suggests that development in the boroughs tends to be concentrated in flood-prone areas. Thus, boroughs may be particularly impacted by the projected increase in flood hazards. This kind of information can be of potential use for borough planning authorities that review regulatory changes in flood hazard zones. Such changes could include, for example, redirecting land development, revisiting flood insurance requirements and/or reducing potential risk by promoting adaptation measures in potential risk zones (Pralle 2019; UNISDR 2015).

Cities and boroughs with highest flood hazards and exposure in current climatic conditions are projected to be roughly the same from future climatic conditions (Fig. 6). In Fig. 6, we show the rank correlation for both flood hazards and exposure between the years 2017 and 2099. The rank correlation for boroughs is shown in Figs. 6a and 6b and cities in Figs. 6c and 6d. We find a strong rank correlation ($R > 0.95$) for both flood hazards and exposure between years 2017 and 2099. This implies that cities and boroughs with high flood hazard and exposure in 2017 are projected to be approximately in the same overall situation in 2099 (Fig. 6). However, the frequency distribution for 2099 indicates a heavy tail for both hazards and exposure (see insets in Fig. 6). Based on the frequency distribution of boroughs and cities for flood hazards and exposure in 2017 and 2099 (Fig. 6), flood risk is projected to increase in 2099 compared to 2017. Also, the number of cities and boroughs with high hazards and exposure is projected to increase in 2099.

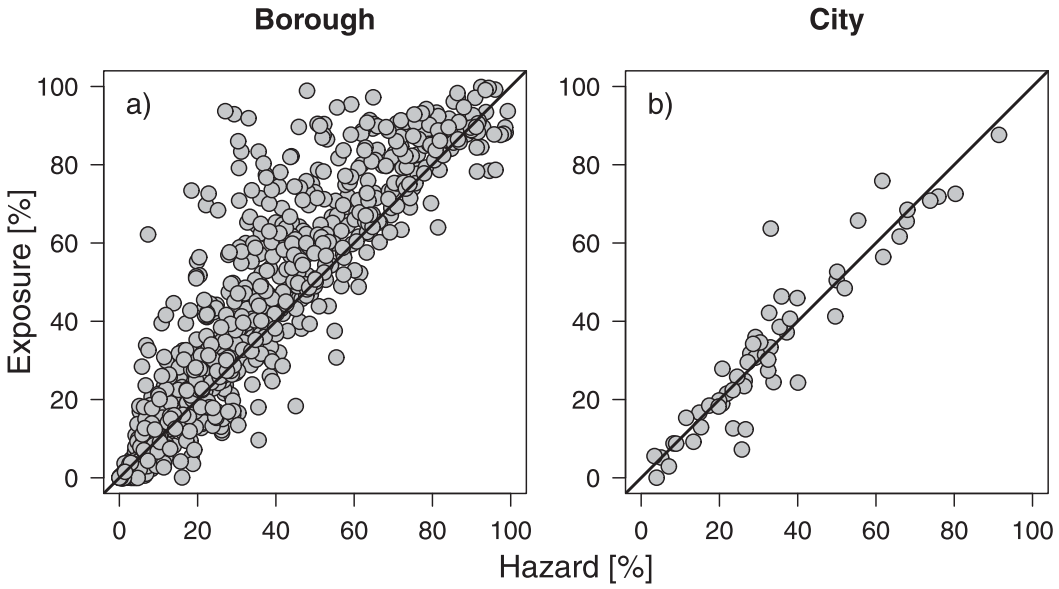

FIG. 5. Correlation between the projected flood hazard and exposure in year 2099 for (a) boroughs and (b) cities. The black line represents the 1:1 fit. Hazard (%) indicates the inundation area standardized to the total area of a city or borough. Exposure (%) indicates the population in the projected flood inundation extents standardized to the total population of a city or borough. The value of the correlation coefficient between hazard and exposure is 0.91 for boroughs and 0.94 for cities.

For instance, the number of boroughs with hazards greater than 60% is projected to increase from 96 in 2017 to 170 in 2099 (Fig. 6a), and in terms of exposure, the number of boroughs is projected to increase from 175 in 2017 to 259 in 2099 (Fig. 6b). Moreover, there is no city with exposure greater than 80% in 2017 (refer inset in Fig. 6d); however, there is one city (Sunbury) with exposure projected to be greater than 80% in 2099.

Our results suggest that flood hazards are increasing under the considered future climate conditions. Changing flood hazards may call for changes in flood-mitigation and flood-adaptation strategies, including floodplain restoration and protection, climate-informed engineering standards, and the use of structural and nonstructural measures (de Moel et al. 2015). These strategies aim to decrease the exposure of people and property to damaging floods by limiting development within high flood risk areas. Indeed, projected flood risk information, such as our flood hazard and exposure metrics, should be valuable to stakeholders (e.g., planners, decision-makers, and engineers) charged with designing and implementing policies and laws at both local and regional level.

Our estimates of flood hazards and exposure do not consider the effects of structural mitigation measures, such as dams and levees, on flood inundation. Dams and levees play an important role in reducing existing flood risk at many locations within Pennsylvania (PIRC 2018). By evaluating scenarios with and without structural mitigation measures, additional valuable information could be provided to stakeholders. However, it should also be recognized that the ability of dams and levees to provide adequate flood protection in the future in unknown, since many of these systems are in need of urgent rehabilitation and investment (PIRC 2018).

d. Uncertainty quantification in flood inundation projections

We use a case study to quantify the contribution of key sources of uncertainties to the projected flood inundation extents. We focus on Selinsgrove, a riverine community along the main stem of the Susquehanna River, with a total area of 4.92 km^2 and a population of 5654 in 2010 (U.S. Census Bureau 2010). Figure 7 compares the 100-yr flood inundation extents in the borough of Selinsgrove based on the stationary flood peak estimate from FEMA, nonstationary flood peak estimate in 2017, and nonstationary flood peak projection for years 2060 and 2099. We find that the FEMA 100-yr flood extent is less than the projected flood hazard under nonstationary conditions in 2017 derived in this study (Fig. 7). Maybe more importantly, the projected flood hazards increase with future projections (Fig. 7).

We quantify both the individual and combined sources of uncertainty in different stages of the flood inundation projection chain, including the climate, hydrologic and hydraulic stage. Figure 8 summarizes the uncertainty quantification results for the 100-yr flood inundation extent in year 2099 using two uncertainty measures: range (Fig. 8a) and standard deviation (Fig. 8b). In Fig. 8, the percentage in the bracket under stage uncertainty indicates the proportion of the uncertainty of each stage contributed to the total uncertainty, while the percentage in the bracket under cumulative uncertainty indicates the proportion of the cumulative uncertainty up to a particular stage.

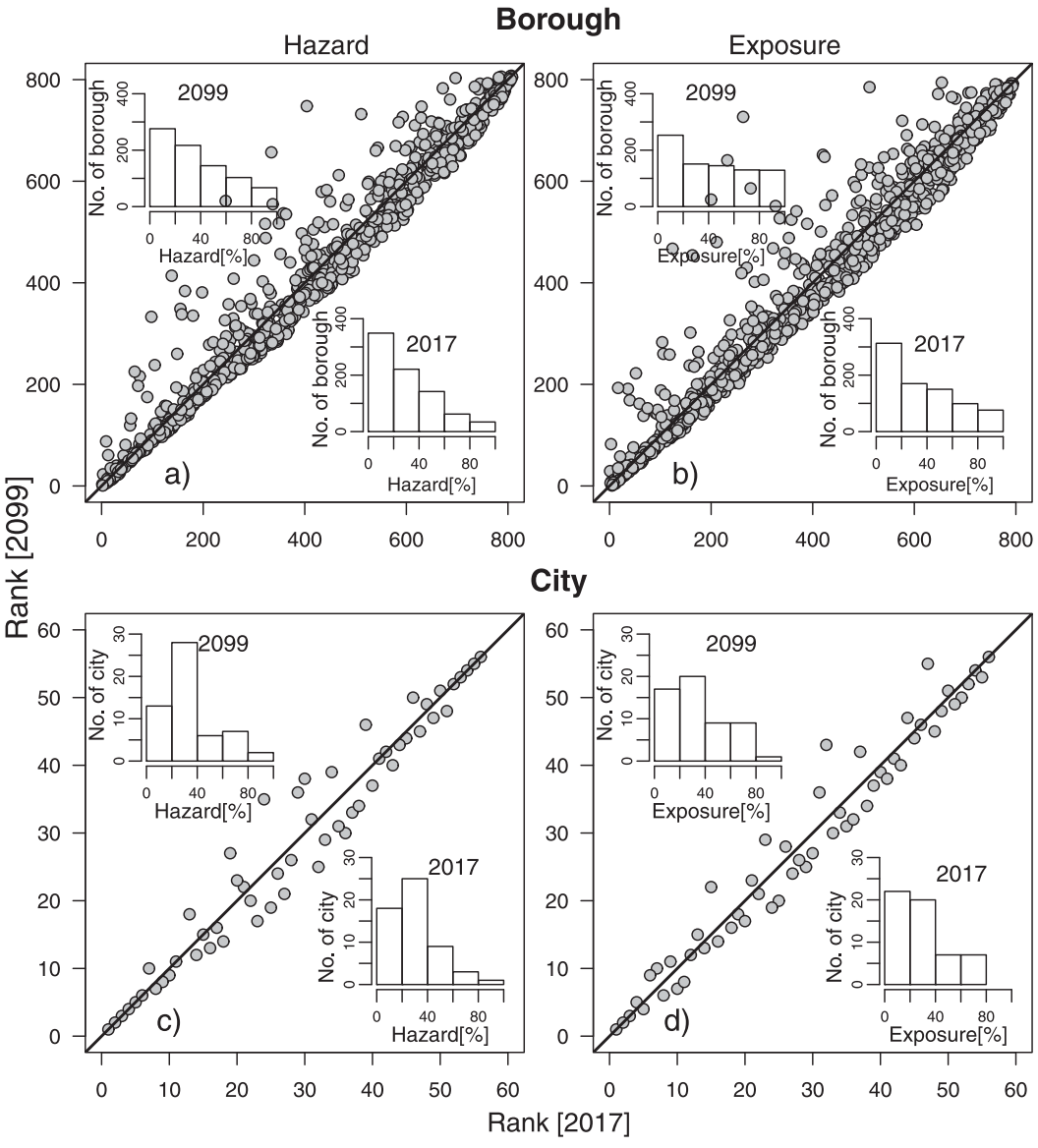

FIG. 6. Rank correlation between years 2017 and 2099 for the flood hazard and exposure of (a),(b) boroughs and (c),(d) cities. The insets show the frequency distribution of standardized flood hazard and exposure for boroughs and cities.

The total range of projected flood inundation extent in Selinsgrove suggested by this analysis is 0.37 km^2, with an inundation extent varying from 2.33 to 2.70 km^2 (Fig. 8a). The range in flood inundation extent by just considering the sampling uncertainties in climate model outputs is 0.23 km^2. Cumulative uncertainty in the hydrologic stage is 0.33 km^2. The cumulative uncertainty in the hydrologic stage is the range of flood inundation extent that considers both climate and hydrologic uncertainties, while keeping the hydraulic stage constant. Thus, the hydrologic stage alone contributes 0.1 km^2 uncertainty in flood inundation extent. The difference between the total uncertainty in the projected flood inundation extents and cumulative uncertainty in hydrologic stage provides the hydraulic stage uncertainty. The range of the projected flood inundation extents due to the hydraulic stage alone is 0.04 km^2.

We analyze the uncertainty decomposition results using two measures—range and standard deviation—and arrive at broadly comparable results (Fig. 8). The effects of the considered climate uncertainty dominate the effects of hydrologic and hydraulic uncertainties for both metrics. For instance, when we use the range of the projected flood inundation extents as the uncertainty measure above 60% of the total uncertainty is contributed by the climate model outputs. Thus, reducing the uncertainty in projections of future climate would make a substantial contribution to reducing overall uncertainty in flood inundation projections. The hydrologic stage

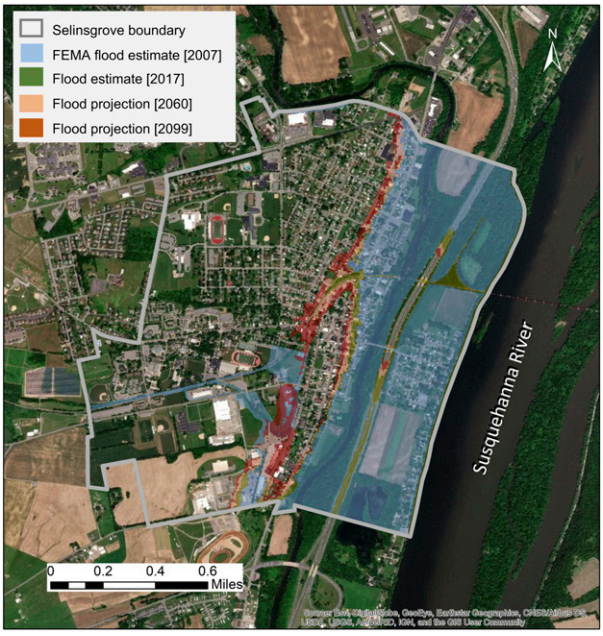

FIG. 7. The 100-yr flood inundation extents in the borough of Selinsgrove, Pennsylvania, using FEMA stationary flood peak estimates (FEMA 2019), nonstationary flood peak estimates in year 2017, and nonstationary flood peak projections for years 2060 and 2099. FEMA = Federal Emergency Management Agency.

comprises the second largest uncertainty source, which accounts for more than 25% of the total uncertainty. The combined contribution of climate and hydrologic uncertainty is about 90% of the total uncertainty. The hydraulic stage alone represents about 10% of the total uncertainty.

Flood inundation projections are uncertain and depend on the magnitudes and interactions of the uncertainties in the different stages (e.g., climate, hydrologic, and hydraulic) of the projection chain. Prior studies addressing sources of uncertainty in flood projections have focused on quantifying the climate and hydrologic uncertainty. These studies provide important insights but are often silent on the relative contribution of hydraulic uncertainty in the flood-inundation projection chain (Bosshard et al. 2013; Qi et al. 2016; Kim et al. 2019). Our results indicate that all of the investigated uncertainty sources (i.e., climate, hydrologic, and hydraulic) make sizeable contributions. Indeed, both uncertainty measures indicate that the hydraulic uncertainty has a nonnegligible influence on the projected flood inundation extent. Neglecting the contribution of hydraulic uncertainty in climate change impact assessment can overestimate the relative importance of climate and hydrologic uncertainties.

4. Summary and conclusions

We design, implement, and test an integrated framework to assess regional riverine flood inundation risks in a changing climate. Regional flood inundation modeling can inform the assessment of flood risk across localities and can identify potential risk hotspots. We focus on a case study for the U.S. state of Pennsylvania where many communities have experienced an increase in the frequency and magnitude of floods and associated damages (Shortle et al. 2020). Although the case study focuses on Pennsylvania, the framework is general and can be applied to other regions.

The proposed framework links climate model outputs, a hydrologic model, a statistical model, and a hydraulic model. In this implementation, we use downscaled climate projections for precipitation and temperature from CMIP5 models to force the National Oceanic and Atmospheric Administration's (NOAA) Hydrology Laboratory-Research Distributed Hydrologic Model (HL-RDHM) and produce streamflow projections. We fit the generalized Pareto distribution (GPD) to the projected streamflow and compute extreme flows with a 100-yr return period. We use the 100-yr flood peak as a boundary condition for the hydraulic model LISFLOOD-FP and to generate flood inundation projections. Finally, the flood inundation projections are used to perform flood hazards and exposure analyses. Our regional flood hazards and exposure assessment for Pennsylvania suggests four main conclusions:

1) Assuming a stationary climate can underestimate regional flood risk.
2) Future flood peak alterations due to climate change are projected to be greater for smaller basins, which capture the spatial scale at which many flood-related infrastructure decisions are made.
3) Most cities and boroughs in Pennsylvania are projected to face higher flood risk under projected future climate conditions. Flood risks are relatively higher in smaller cities and boroughs compared to the largest cities. However, the cities and boroughs with highest flood risk in 2017 are projected to be roughly the same in 2099.
4) Climate uncertainty is the dominant contributor to flood hazard uncertainties. The hydrologic stage is the second largest uncertainty source. We also find that hydraulic uncertainty has an important influence on extreme flood uncertainty. Neglecting the contribution of hydraulic uncertainty to the total uncertainty in climate change impact assessment could lead to overconfident estimates of flood hazard uncertainty.

This study provides an integrated, multimodel and multiscale framework to develop local-to-regional-scale flood-risk information in a changing climate. Avenues for future work to overcome limitations in our study include (i) the explicit inclusion of relevant physical infrastructure in the hydrologic and hydraulic model, and (ii) a more comprehensive uncertainty quantification by incorporating additional sources of uncertainties, including different emission and land use cover scenarios, climate and hydrologic models, downscaling approaches, sets of hydrologic and hydraulic model parameters, and channel boundary conditions (e.g., channel geometry, erosion and sediment deposition). Given the substantial power of adaptation and mitigation measures to reduce flood hazards and exposures, our results approximate the upper envelope of possible flood risks.

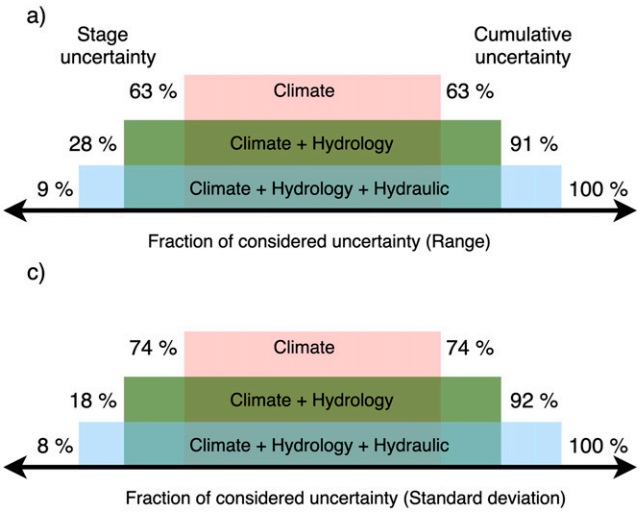

b) Projected flood inundation (Range, km^2)

Stage	Cumulative uncertainty	Stage uncertainty
Climate	0.23	0.23
Hydrology	0.33	0.10
Hydraulic	0.37	0.04

d) Projected flood inundation (Standard deviation)

Stage	Cumulative uncertainty	Stage uncertainty
Climate	0.026	0.026
Hydrology	0.032	0.006
Hydraulic	0.035	0.0026

FIG. 8. Decomposition of the uncertainty in the projected flood inundation extents for year 2099 using two different measures: (a),(b) range and (c),(d) standard deviation. The individual and combined sources of uncertainties (climate, hydrology, and hydraulics) in the flood inundation projection chain are shown. In (a) and (c) the percentage values under stage uncertainty indicate the proportion of the uncertainty that each stage contributes to the total uncertainty; the percentage values under cumulative uncertainty indicate the proportion of the cumulative uncertainty up to that particular stage. The individual stage uncertainty and cumulative uncertainties up to the corresponding stage are shown using range in (b) and standard deviation in (d).

For making real-world decisions, more detailed studies are needed that account for adaptation and mitigation measures, such as the effect of dams and levees on flood risk.

Acknowledgments. This work was supported through the Penn State Initiative for Resilient Communities (PSIRC) by a Strategic Plan seed grant from the Penn State Office of the Provost, with co-support from the Center for Climate Risk Management (CLIMA), the Rock Ethics Institute, Penn State Law, the Hamer Center for Community Design, and by the National Oceanic and Atmospheric Administration through the Mid-Atlantic Regional Integrated Sciences and Assessments (MARISA) program under NOAA Grant NA16OAR4310179. All errors and opinions are from the authors and do not reflect the funding agencies. We are grateful to Lisa Iulo, James Ross-Golin, Lara Fowler, Skip Wishbone, and Irene Schaperdoth for their helpful feedback and advice. The authors declare no competing financial or nonfinancial interests. This is academic research and not designed to be used in actual decision-making. The code and data used for this analysis is available at GitHub repository: https://github.com/svs6308/Flood-Hazard-Projection, under the GNU general public open source license. The results, data, software tools, and other resources related to this work are provided as-is without warranty of any kind, expressed or implied. In no event shall the authors or copyright holders be liable for any claim, damages, or other liability in connection with the use of these resources.

REFERENCES

Aich, V., and Coauthors, 2016: Flood projections within the Niger River Basin under future land use and climate change. *Sci. Total Environ.*, **562**, 666–677, https://doi.org/10.1016/j.scitotenv.2016.04.021.

Alfieri, L., L. Feyen, F. Dottori, and A. Bianchi, 2015: Ensemble flood risk assessment in Europe under high end climate scenarios. *Global Environ. Change*, **35**, 199–212, https://doi.org/10.1016/j.gloenvcha.2015.09.004.

——, B. Bisselink, F. Dottori, G. Naumann, A. Roo, P. Salamon, K. Wyser, and L. Feyen, 2017: Global projections of river flood risk in a warmer world. *Earth's Future*, **5**, 171–182, https://doi.org/10.1002/2016EF000485.

Alfonso, L., M. M. Mukolwe, and G. Di Baldassarre, 2016: Probabilistic flood maps to support decision-making: Mapping the value of information. *Water Resour. Res.*, **52**, 1026–1043, https://doi.org/10.1002/2015WR017378.

Armstrong, W. H., M. J. Collins, and N. P. Snyder, 2014: Hydroclimatic flood trends in the northeastern United States and linkages with large-scale atmospheric circulation patterns. *Hydrol. Sci. J.*, **59**, 1636–1655, https://doi.org/10.1080/02626667.2013.862339.

Arnell, N. W., and S. N. Gosling, 2014: The impacts of climate change on river flood risk at the global scale. *Climatic Change*, **134**, 387–401, https://doi.org/10.1007/s10584-014-1084-5.

Bales, J. D., and C. R. Wagner, 2009: Sources of uncertainty in flood inundation maps. *J. Flood Risk Manag.*, **2**, 139–147, https://doi.org/10.1111/j.1753-318X.2009.01029.x.

Bates, P. D., M. Trigg, J. Neal, and A. Dabrowa, 2013: LISFLOOD-FP. User manual. School of Geographical Sciences, University of Bristol, 49 pp., https://www.bristol.ac.uk/media-library/sites/geography/migrated/documents/lisflood-manual-v5.9.6.pdf.

——, and Coauthors, 2021: Combined modelling of US fluvial, pluvial, and coastal flood hazard under current and future climates. *Water Resour. Res.*, **57**, e2020WR028673, https://doi.org/10.1029/2020WR028673.

Bopp, G. P., B. A. Shaby, C. E. Forest, and A. Mejía, 2020: Projecting flood-inducing precipitation with a Bayesian

analogue model. *J. Agric. Biol. Environ. Stat.*, **25**, 229–249, https://doi.org/10.1007/s13253-020-00391-6.

Bosshard, T., M. Carambia, K. Goergen, S. Kotlarski, P. Krahe, M. Zappa, and C. Schär, 2013: Quantifying uncertainty sources in an ensemble of hydrological climate-impact projections. *Water Resour. Res.*, **49**, 1523–1536, https://doi.org/10.1029/2011WR011533.

Bracken, C., K. D. Holman, B. Rajagopalan, and H. Moradkhani, 2018: A Bayesian hierarchical approach to multivariate nonstationary hydrologic frequency analysis. *Water Resour. Res.*, **54**, 243–255, https://doi.org/10.1002/2017WR020403.

Brooks, L. T., 2005: Flood of September 18–19, 2004 in the upper Delaware River basin. USGS Open-File Rep. 2005-1166, 123 pp., https://pubs.er.usgs.gov/publication/ofr20051166.

Chaplin, J. J., 2005: Development of regional curves relating bankfull-channel geometry and discharge to drainage area for streams in Pennsylvania and selected areas of Maryland. USGS Scientific Investigations Rep. 2005-5147, 34 pp., http://pubs.usgs.gov/sir/2005/5147/.

Chen, J., F. P. Brissette, A. Poulin, and R. Leconte, 2011: Overall uncertainty study of the hydrological impacts of climate change for a Canadian watershed. *Water Resour. Res.*, **47**, W12509, https://doi.org/10.1029/2011WR010602.

Cheng, C., Y. E. Yang, R. Ryan, Q. Yu, and E. Brabec, 2017: Assessing climate change-induced flooding mitigation for adaptation in Boston's Charles River watershed, USA. *Landscape Urban Plann.*, **167**, 25–36, https://doi.org/10.1016/j.landurbplan.2017.05.019.

Cinotto, P. J., 2003: Development of regional curves of bankfull-channel geometry and discharge for streams in the non-urban, Piedmont Physiographic Province, Pennsylvania and Maryland (No. 3). USGS Water-Resources Investigations Rep. 2003-4014, 27 pp., http://pubs.er.usgs.gov/publication/wri034014.

Clune, J. W., J. J. Chaplin, and K. E. White, 2018: Comparison of regression relations of bankfull discharge and channel geometry for the glaciated and nonglaciated settings of Pennsylvania and southern New York (ver. 1.1, July 2020). USGS Scientific Investigations Rep. 2018-5066, 20 pp., https://pubs.er.usgs.gov/publication/sir20185066.

Coles, S. G., 2001: *An Introduction to Statistical Modeling of Extreme Values*. Springer, 225 pp.

Collet, L., L. Beevers, and M. D. Stewart, 2018: Decision-making and flood risk uncertainty: Statistical data set analysis for flood risk assessment. *Water Resour. Res.*, **54**, 7291–7308, https://doi.org/10.1029/2017WR022024.

de Moel, H., B. Jongman, H. Kreibich, B. Merz, E. Penning-Rowsell, and P. J. Ward, 2015: Flood risk assessments at different spatial scales. *Mitigation Adapt. Strategies Global Change*, **20**, 865–890, https://doi.org/10.1007/s11027-015-9654-z.

Demaria, E. M., R. N. Palmer, and J. K. Roundy, 2016: Regional climate change projections of streamflow characteristics in the Northeast and Midwest US. *J. Hydrol. Reg. Stud.*, **5**, 309–323, https://doi.org/10.1016/j.ejrh.2015.11.007.

Dibike, Y. B., and P. Coulibaly, 2005: Hydrologic impact of climate change in the Saguenay watershed: Comparison of downscaling methods and hydrologic models. *J. Hydrol.*, **307**, 145–163, https://doi.org/10.1016/j.jhydrol.2004.10.012.

Dobler, C., G. Bürger, and J. Stötter, 2012: Assessment of climate change impacts on flood hazard potential in the Alpine Lech watershed. *J. Hydrol.*, **460**, 29–39, https://doi.org/10.1016/j.jhydrol.2012.06.027.

DRBC, 2006: Flooding events in the Delaware River basin. Delaware River Basin Commission, accessed July 2019, https://www.state.nj.us/drbc/hydrological/flood/drb-flood-events.html.

England, J. F., Jr., T. A. Cohn, B. A. Faber, J. R. Stedinger, W. O. Thomas Jr., A. G. Veilleux, J. E. Kiang, and R. R. Mason Jr., 2018: Guidelines for determining flood flow frequency. USGS Bull. 17C, Techniques and Methods 4-B5, 148 pp., https://pubs.usgs.gov/tm/04/b05/tm4b5.pdf.

FCSMA, 2020: Flood history. Flood Control Sunbury Municipal Authority, http://sunburyfloodcontrol.com/flood-history.html.

FEMA, 2019: Flood Insurance Rate Map (FIRM). Federal Emergency Management Agency, https://www.fema.gov/flood-insurance-rate-map-firm.

Feyen, L., R. Dankers, K. Bódis, P. Salamon, and J. I. Barredo, 2012: Fluvial flood risk in Europe in present and future climates. *Climatic Change*, **112**, 47–62, https://doi.org/10.1007/s10584-011-0339-7.

FSF, 2020: The first national flood risk assessment: Defining America's growing risk. The First Street Foundation, 163 pp., https://assets.firststreet.org/uploads/2020/06/first_street_foundation__first_national_flood_risk_assessment.pdf.

Gangrade, S., S. C. Kao, and R. A. McManamay, 2020: Multimodel Hydroclimate projections for the Alabama-Coosa-Tallapoosa River Basin in the southeastern United States. *Sci. Rep.*, **10**, 2870, https://doi.org/10.1038/s41598-020-59806-6.

Gitro, C. M., M. S. Evan, and R. H. Grumm, 2014: Two major heavy rain/flood events in the Mid-Atlantic: June 2006 and September 2011. *J. Operat. Meteor.*, **2**, 152–168, https://doi.org/10.15191/nwajom.2014.0213.

Gomez, M., S. Sharma, S. Reed, and A. Mejia, 2019: Skill of ensemble flood inundation forecasts at short-to medium-range timescales. *J. Hydrol.*, **568**, 207–220, https://doi.org/10.1016/j.jhydrol.2018.10.063.

Gori, A., N. Lin and J. Smith, 2020: Assessing compound flooding from landfalling tropical cyclones on the North Carolina coast. *Water Resour. Res.*, **56**, e2019WR026788, https://doi.org/10.1029/2019WR026788.

Hattermann, F. F., and Coauthors, 2017: Cross-scale intercomparison of climate change impacts simulated by regional and global hydrological models in eleven large river basins. *Climatic Change*, **141**, 561–576, https://doi.org/10.1007/s10584-016-1829-4.

Hayhoe, K., and Coauthors, 2018: Our changing climate. *Impacts, Risks, and Adaptation in the United States: Fourth National Climate Assessment*, *Volume II*, D. R. Reidmiller et al., Eds., U.S. Global Change Research Program, 72–144.

Hirabayashi, Y., R. Mahendran, S. Koirala, L. Konoshima, D. Yamazaki, S. Watanabe, H. Kim, and S. Kanaes, 2013: Global flood risk under climate change. *Nat. Climate Change*, **3**, 816–821, https://doi.org/10.1038/nclimate1911.

Homer, C. H., J. A. Fry, and C. A. Barnes, 2012: The National Land Cover Database. USGS Fact Sheet 2012–3020, 4 pp., https://www.usgs.gov/centers/eros/science/national-land-cover-database?qt-science_center_objects=0#qt-science_center_objects.

Huang, S., F. F. Hattermann, V. Krysanova, and A. Bronstert, 2013: Projections of climate change impacts on river flood conditions in Germany by combining three different RCMs with a regional eco-hydrological model. *Climatic Change*, **116**, 631–663, https://doi.org/10.1007/s10584-012-0586-2.

Iulo, L., and Coauthors, 2020: Establishing priorities for Pennsylvania community flood resilience. PSIRC, 7 pp., accessed 17 September 2020, https://www.psirc.psu.edu/misc/Iulo_etal_2020.Establishing_Priorities_White_Paper.pdf.

Jongman, B., and Coauthors, 2015: Declining vulnerability to river floods and the global benefits of adaptation. *Proc. Natl. Acad. Sci. USA*, **112**, E2 271–E2 280, https://doi.org/10.1073/pnas.1414439112.

Jovanovic, T., A. Mejía, H. Gall, and J. Gironás, 2016: Effect of urbanization on the long-term persistence of streamflow records. *Physica A*, **447**, 208–221, https://doi.org/10.1016/j.physa.2015.12.024.

——, S. García, H. Gall, and A. Mejía, 2017: Complexity as a streamflow metric of hydrologic alteration. *Stochastic Environ. Res. Risk Assess.*, **31**, 2107–2119, https://doi.org/10.1007/s00477-016-1315-6.

——, F. Sun, T. Mahjabin, and A. Mejia, 2018: Disentangling the effects of climate and urban growth on streamflow for sustainable urban development: A stochastic approach to flow regime attribution. *Landscape Urban Plann.*, **177**, 160–170, https://doi.org/10.1016/j.landurbplan.2018.05.009.

Judi, D. R., C. L. Rakowski, S. R. Waichler, Y. Feng, and M. S. Wigmosta, 2018: Integrated modeling approach for the development of climate-informed, actionable information. *Water*, **10**, 775, https://doi.org/10.3390/w10060775.

Kang, H., and V. Sridhar, 2018: Assessment of future drought conditions in the Chesapeake Bay watershed. *J. Amer. Water Resour. Assoc.*, **54**, 160–183, https://doi.org/10.1111/1752-1688.12600.

Keller, K., C. Helgeson, and V. Srikrishnan, 2020: Climate risk management. *Annu. Rev. Earth Planet. Sci.*, **49**, 95–116, https://doi.org/10.1146/annurev-earth-080320-055847.

Kim, Y., I. Ohn, J. K. Lee, and Y. O. Kim, 2019: Generalizing uncertainty decomposition theory in climate change impact assessments. *J. Hydrol. X*, **3**, 100024, https://doi.org/10.1016/j.hydroa.2019.100024.

Knutson, T. R., J. J. Sirutis, M. Zhao, R. E. Tuleya, M. Bender, G. A. Vecchi, G. Villarini, and D. Chavas, 2015: Global projections of intense tropical cyclone activity for the late 21st century from dynamical downscaling of CMIP5/RCP4.5 scenarios. *J. Climate*, **28**, 7203–7224, https://doi.org/10.1175/JCLI-D-15-0129.1.

Koren, V., S. Reed, M. Smith, Z. Zhang, and D.-J. Seo, 2004: Hydrology Laboratory Research Modeling System (HL-RMS) of the US National Weather Service. *J. Hydrol.*, **291**, 297–318, https://doi.org/10.1016/j.jhydrol.2003.12.039.

Koutsoyiannis, D., 2006: Nonstationarity versus scaling in hydrology. *J. Hydrol.*, **324**, 239–254, https://doi.org/10.1016/j.jhydrol.2005.09.022.

Kundzewicz, Z. W., D. L. T. Hegger, P. Matczak, and P. P. J. Driessen, 2018: Opinion: Flood-risk reduction: Structural measures and diverse strategies. *Proc. Natl. Acad. Sci. USA*, **115**, 12 321–12 325, https://doi.org/10.1073/pnas.1818227115.

Kuzmin, V. A., 2009: Algorithms of automatic calibration of multiparameter models used in operational systems of flash flood forecasting. *Russ. Meteor. Hydrol.*, **34**, 473–481, https://doi.org/10.3103/S1068373909070073.

——, D.-J. Seo, and V. Koren, 2008: Fast and efficient optimization of hydrologic model parameters using a priori estimates and stepwise line search. *J. Hydrol.*, **353**, 109–128, https://doi.org/10.1016/j.jhydrol.2008.02.001.

Lang, M., T. Ouarda, and B. Bobée, 1999: Towards operational guidelines for over-threshold modeling. *J. Hydrol.*, **225**, 103–117, https://doi.org/10.1016/S0022-1694(99)00167-5.

Lin, S., C. Jing, N. A. Coles, V. Chaplot, N. J. Moore, and J. Wu, 2013: Evaluating DEM source and resolution uncertainties in the Soil and Water Assessment Tool. *Stochastic Environ. Res. Risk Assess.*, **27**, 209–221, https://doi.org/10.1007/s00477-012-0577-x.

McCuen, R. H., and W. M. Snyder, 1975: A proposed index for comparing hydrographs. *Water Resour. Res.*, **11**, 1021–1024, https://doi.org/10.1029/WR011i006p01021.

Meinshausen, M., and Coauthors, 2011: The RCP greenhouse gas concentrations and their extensions from 1765 to 2300. *Climatic Change*, **109**, 213–241, https://doi.org/10.1007/s10584-011-0156-z.

Mejia, A. I., and S. M. Reed, 2011a: Role of channel and floodplain cross-section geometry in the basin response. *Water Resour. Res.*, **47**, W09518, https://doi.org/10.1029/2010WR010375.

——, and ——, 2011b: Evaluating the effects of parameterized cross section shapes and simplified routing with a coupled distributed hydrologic and hydraulic model. *J. Hydrol.*, **409**, 512–524, https://doi.org/10.1016/j.jhydrol.2011.08.050.

Merwade, V., F. Olivera, M. Arabi, and S. Edleman, 2008: Uncertainty in flood inundation mapping: Current issues and future directions. *J. Hydrol. Eng.*, **13**, 608–620, https://doi.org/10.1061/(ASCE)1084-0699(2008)13:7(608).

Merwade, V. M., D. R. Maidment, and J. A. Goff, 2006: Anisotropic considerations while interpolating river channel bathymetry. *J. Hydrol.*, **331**, 731–741, https://doi.org/10.1016/j.jhydrol.2006.06.018.

Nash, J. E., and J. V. Sutcliffe, 1970: River flow forecasting through conceptual models part I – A discussion of principles. *J. Hydrol.*, **10**, 282–290, https://doi.org/10.1016/0022-1694(70)90255-6.

NCEI, 2020: Storm events database. NOAA/NCEI, https://www.ncdc.noaa.gov/stormevents/.

Neal, J., I. Villanueva, N. Wright, T. Willis, T. Fewtrell, and P. D. Bates, 2012: How much physical complexity is needed to model flood inundation? *Hydrol. Processes*, **26**, 2264–2282, https://doi.org/10.1002/hyp.8339.

Newlin, J. T., and B. R. Hayes, 2015: Hydraulic modeling of glacial dam-break floods on the West Branch of the Susquehanna River, Pennsylvania. *Earth Space Sci.*, **2**, 229–243, https://doi.org/10.1002/2015EA000096.

Papoulis, A., and S. U. Pillai, 2002: *Probability, Random Variables, and Stochastic Processes*. McGraw-Hill, 852 pp.

Pappenberger, F., K. Beven, M. Horritt, and S. Blazkova, 2005: Uncertainty in the calibration of effective roughness parameters in HEC-RAS using inundation and downstream level observations. *J. Hydrol.*, **302**, 46–69, https://doi.org/10.1016/j.jhydrol.2004.06.036.

——, P. Matgen, K. J. Beven, J. B. Henry, and L. Pfister, 2006: Influence of uncertain boundary conditions and model structure on flood inundation predictions. *Adv. Water Resour.*, **29**, 1430–1449, https://doi.org/10.1016/j.advwatres.2005.11.012.

PEMA, 2017: Summary of commonwealth vulnerability analysis. PEMA, https://www.pema.pa.gov/Floodplain-Management/Pages/default.aspx.

Pierce, D. W., D. R. Cayan, and B. L. Thrasher, 2014: Statistical downscaling using localized constructed analogs (LOCA). *J. Hydrometeor.*, **15**, 2558–2585, https://doi.org/10.1175/JHM-D-14-0082.1.

PIRC, 2018: Pennsylvania infrastructure report card. Accessed 25 May 2018, https://infrastructurereportcard.org/state-item/pennsylvania/.

Pralle, S., 2019: Drawing lines: FEMA and the politics of mapping flood zones. *Climatic Change*, **152**, 227–237, https://doi.org/10.1007/s10584-018-2287-y.

Prat, O. P., and B. R. Nelson, 2015: Evaluation of precipitation estimates over CONUS derived from satellite, radar, and rain gauge data sets at daily to annual scales (2002–2012). *Hydrol. Earth Syst. Sci.*, **19**, 2037–2056, https://doi.org/10.5194/hess-19-2037-2015.

Qi, W., C. Zhang, G. Fu, H. Zhou, and J. Liu, 2016: Quantifying uncertainties in extreme flood predictions under climate change for a medium-sized basin in northeastern China. *J. Hydrometeor.*, **17**, 3099–3112, https://doi.org/10.1175/JHM-D-15-0212.1.

Reed, S., V. Koren, M. Smith, Z. Zhang, F. Moreda, D.-J. Seo, and D. Participants, 2004: Overall distributed model intercomparison project results. *J. Hydrol.*, **298**, 27–60, https://doi.org/10.1016/j.jhydrol.2004.03.031.

Roland, M. A., and S. A. Hoffman, 2011: Development of flood-inundation maps for the West Branch Susquehanna River near the Borough of Jersey Shore, Lycoming County, Pennsylvania. USGS Scientific Investigations Rep. 2010–5057, 9 pp., https://pubs.er.usgs.gov/publication/sir20105057.

Ruhi, A., M. L. Messager, and J. D. Olden, 2018: Tracking the pulse of the Earth's fresh waters. *Nat. Sustainability*, **1**, 198–203, https://doi.org/10.1038/s41893-018-0047-7.

Sagarika, S., A. Kalra, and S. Ahmad, 2014: Evaluating the effect of persistence on long-term trends and analyzing step changes in streamflows of the continental United States. *J. Hydrol.*, **517**, 36–53, https://doi.org/10.1016/j.jhydrol.2014.05.002.

Sanders, B. F., and Coauthors, 2020: Collaborative modeling with fine-resolution data enhances flood awareness, minimizes differences in flood perception, and produces actionable flood maps. *Earth's Future*, **7**, e2019EF001391, https://doi.org/10.1029/2019EF001391.

Sharma, S., R. Siddique, S. Reed, P. Ahnert, P. A. Mendoza Zúñiga, and A. Mejia, 2018: Relative effects of statistical preprocessing and postprocessing on a regional hydrological ensemble prediction system. *Hydrol. Earth Syst. Sci.*, **22**, 1831–1849, https://doi.org/10.5194/hess-22-1831-2018.

Shortle, J., and Coauthors, 2015: Pennsylvania Climate Impacts Assessment Update. Pennsylvania Department of Environmental Protection, 199 pp., https://www.dep.pa.gov/Citizens/climate/Pages/impacts.aspx.

——, and Coauthors, 2020: Pennsylvania Climate Impacts Assessment Update. Pennsylvania Department of Environmental Protection, 149 pp., https://www.dep.pa.gov/Citizens/climate/Pages/impacts.aspx.

Siddique, R., and A. Mejia, 2017: Ensemble streamflow forecasting across the U.S. Mid-Atlantic region with a distributed hydrological model forced by GEFS reforecasts. *J. Hydrometeor.*, **18**, 1905–1928, https://doi.org/10.1175/JHM-D-16-0243.1.

Smith, J. A., M. L. Baeck, G. Villarini, and W. F. Krajewski, 2010: The hydrology and hydrometeorology of flooding in the Delaware River basin. *J. Hydrometeor.*, **11**, 841–859, https://doi.org/10.1175/2010JHM1236.1.

——, G. Villarini, and M. L. Baeck, 2011: Mixture distributions and the hydroclimatology of extreme rainfall and flooding in the eastern United States. *J. Hydrometeor.*, **12**, 294–309, https://doi.org/10.1175/2010JHM1242.1.

Smith, M. B., and Coauthors, 2012: The distributed model intercomparison project—Phase 2: Motivation and design of the Oklahoma experiments. *J. Hydrol.*, **418–419**, 3–16, https://doi.org/10.1016/j.jhydrol.2011.08.055.

Sorribas, M. V., and Coauthors, 2016: Projections of climate change effects on discharge and inundation in the Amazon basin. *Climatic Change*, **136**, 555–570, https://doi.org/10.1007/s10584-016-1640-2.

Srikrishnan, V., R. Alley, and K. Keller, 2019: Investing in science to improve climate risk management. *Eos, Trans. Amer. Geophys. Union*, **100**, https://doi.org/10.1029/2019EO131077.

Sriver, R. L., C. E. Forest, and K. Keller, 2015: Effects of initial conditions uncertainty on regional climate variability: An analysis using a low-resolution CESM ensemble. *Geophys. Res. Lett.*, **42**, 5468–5476, https://doi.org/10.1002/2015GL064546.

Stephenson, A., and J. Tawn, 2004: Bayesian inference for extremes: Accounting for the three extremal types. *Extremes*, **7**, 291–307, https://doi.org/10.1007/s10687-004-3479-6.

Strachan, J., P. L. Vidale, K. Hodges, M. Roberts, and M.-E. Demory, 2013: Investigating global tropical cyclone activity with a hierarchy of AGCMs: The role of model resolution. *J. Climate*, **26**, 133–152, https://doi.org/10.1175/JCLI-D-12-00012.1.

Suro, T. P., G. D. Firda, and C. O. Szabo, 2009: Flood of June 26–29, 2006, Mohawk, Delaware, and Susquehanna River basins. USGS Open-File Rep. 2009–1063, 354 pp., http://pubs.usgs.gov/ofr/2009/1063.

Taylor, K. E., R. J. Stouffer, and G. A. Meehl, 2012: An overview of CMIP5 and the experiment design. *Bull. Amer. Meteor. Soc.*, **93**, 485–498, https://doi.org/10.1175/BAMS-D-11-00094.1.

UNISDR, 2015: Making Development Sustainable: The Future of Disaster Risk Management. Global Assessment Report on Disaster Risk Reduction, 316 pp., www.unisdr.org/we/inform/publications/42809.

U.S. Census Bureau, 2010: Census, profile of general population and housing characteristics: 2010 demographic profile data, Table DP-1, https://www.census.gov/library/publications/2012/dec/cph-1.html.

USDOE, 2015: State of Pennsylvania energy sector risk profile. U.S. Department of Energy, https://www.energy.gov/sites/prod/files/2015/05/f22/PA-Energy%20Sector%20Risk%20Profile.pdf.

Varis, O., T. Kajander, and R. Lemmelä, 2004: Climate and water: From climate models to water resources management and vice versa. *Climatic Change*, **66**, 321–344, https://doi.org/10.1023/B:CLIM.0000044622.42657.d4.

Vetter, T., and Coauthors, 2017: Evaluation of sources of uncertainty in projected hydrological changes under climate change in 12 large-scale river basins. *Climatic Change*, **141**, 419–433, https://doi.org/10.1007/s10584-016-1794-y.

Villarini, G., J. A. Smith, F. Serinaldi, J. Bales, P. D. Bates, and W. F. Krajewski, 2009: Flood frequency analysis for nonstationary annual peak records in an urban drainage basin. *Adv. Water Resour.*, **32**, 1255–1266, https://doi.org/10.1016/j.advwatres.2009.05.003.

Ward, P. J., and Coauthors, 2015: Usefulness and limitations of global flood risk models. *Nat. Climate Change*, **5**, 712–715, https://doi.org/10.1038/nclimate2742.

Wing, O. E. J., P. D. Bates, A. M. Smith, C. C. Sampson, K. A. Johnson, J. Fargione, and P. Morefield, 2018: Estimates of present and future flood risk in the conterminous United States. *Environ. Res. Lett.*, **13**, 034023, https://doi.org/10.1088/1748-9326/aaac65.

Winsemius, H. C., and Coauthors, 2016: Global drivers of future river flood risk. *Nat. Climate Change*, **6**, 381–385, https://doi.org/10.1038/nclimate2893.

Wu, C., G. Huang, H. Yu, Z. Chen, and J. Man, 2014: Impact of climate change on reservoir flood control in the upstream area of the Beijiang River basin, South China. *J. Hydrometeor.*, **15**, 2203–2218, https://doi.org/10.1175/JHM-D-13-0181.1.

Zarekarizi, M., V., Srikrishnan, and K. Keller, 2020: Neglecting uncertainties biases house-elevation decisions to manage riverine flood risks. *Nat. Commun.*, **11**, 5361, https://doi.org/10.1038/s41467-020-19188-9.

Zarzar, C. M., H. Hosseiny, R. Siddique, M. Gomez, V. Smith, A. Mejia, and J. Dyer, 2018: A hydraulic multimodel ensemble framework for visualizing flood inundation uncertainty. *J. Amer. Water Resour. Assoc.*, **54**, 807–819, https://doi.org/10.1111/1752-1688.12656.

Zhang, Z., A. D. Dehoff, R. D. Pody, and J. W. Balay, 2010: Detection of streamflow change in the Susquehanna River Basin. *Water Resour. Manage.*, **24**, 1947–1964, https://doi.org/10.1007/s11269-009-9532-0.